Chapter 1

Advances in Understanding Reactivity of Manganese Oxides with Arsenic and Chromium in Environmental Systems

J. S. Fischel, M. H. Fischel, and D. L. Sparks*

Department of Plant and Soil Sciences, Delaware Environmental Institute, ISE Lab, 221 Academy Street, Suite 250, University of Delaware, Newark, Delaware 19716
***E-mail: dlsparks@udel.edu**

In the past several years, through the use of molecular scale techniques, particularly those that are in-situ, advances have been made in determining the reactivity of manganese oxides with arsenic (As) and chromium (Cr). Of particular note is an enhanced understanding of the kinetics and mechanisms of As(III) and Cr(III) oxidation on Mn-oxides over a range of time scales, from milliseconds to days. This is in large part due to the employment of novel, synchrotron-based techniques, such as Quick X-ray absorption spectroscopy (Q-XAS) and bench-scale attentuated total reflectance Fourier transform infrared (ATR-FTIR) spectroscopy. This review will focus on these advances, and rely heavily on the published research of Sparks and his group, both present and former members. Undoubtedly these advancess were greatly facilitated by a large number of previous investigations by numerous authors, some of which are cited in the review.

Manganese Oxide Reactivity with Arsenic

Manganese-oxide minerals (Mn-oxides) are robust oxidizing agents that play an important role in many redox processes in the natural environment, such as oxidation of arsenic (As) (*1*). Previous studies have suggested that many Mn-oxides found in terrestrial environments are poorly-crystalline and biogenic (*2*, *3*) and extremely reactive (*3*). The reactivity of Mn-oxide minerals depends on

In Advances in the Environmental Biogeochemistry of Manganese Oxides; Sparks, et al.;
ACS Symposium Series; American Chemical Society: Washington, DC, 2015.

their mineralogy. Layered Mn-oxide minerals (i.e. phyllomanganates) are more reactive oxidizing As^{III} than other types of Mn-oxides (*4–8*).

Arsenic (As) is a toxic element in the environment, originating from both geogenic and anthropogenic sources. Its toxicity and mobility are determined by its speciation or form. Arsenite (As^{III}) is more toxic than arsenate (As^{V}) (*9*), and the sorption of As on oxide minerals depends on pH and speciation (*10*, *11*). Manganese-oxides, including phyllomanganates, can oxidize As^{III} to As^{V} (*5–8*, *12–14*), and since As^{III} is more toxic than As^{V} the oxidation process helps detoxify As in the environment. Additionally, As^{III} oxidation by Mn-oxides can decrease the mobility of As mobility (*10*, *15*).

Mechanisms of As^{III} oxidation by Mn-oxides are complex, involving several simultaneous reactions. For example, As^{III} oxidation by birnessite produces As^{V} and Mn^{II} as products. Both As^{V} and Mn^{II} can be adsorbed by birnessite (*4*, *5*). A Mn^{III} intermediate also can form during As^{III} oxidation by Mn-oxides (*7*, *16*). During the reaction with As^{III}, phyllomanganates become passivated, i.e. As^{III} oxidization initially proceeds rapidly, after which there is a decrease in oxidation rate (*5–7*, *12–14*, *17*, *18*). Two potential mechanisms for Mn-oxide passivation are possible. One is the sorption of Mn^{II}, produced by reduction of Mn^{IV} in the mineral structure, which serves to block reactive sites on the mineral surface (*5*, *18*, *19*). A second mechanism is the formation of Mn^{III} on Mn-oxide surfaces, which while less reactive than Mn^{IV} sites, can decrease the As^{III} oxidation rate (*7*, *16*, *20*).

In previous studies passivation of the Mn-oxide surface (represented by $>Mn^{IV}O_2$ in Equation 1) was attributed to sorption of Mn^{II} (Equation 1), which forms during As^{III} oxidation (Equation 2) (*1*, *5*). A Mn^{III} intermediate, produced during As^{III} oxidation by phyllomanganates (*16*), is thought to be another cause of Mn-oxide passivation (Equations 3 and 4) (*7*, *16*).

$$Mn^{II} + >Mn^{IV}O_2 \rightarrow >Mn^{IV}O_2\text{-}Mn^{II} \quad [1]$$

$$Mn^{IV}O_2 + H_3As^{III}O_3 + H^+ \rightarrow Mn^{II} + H_2As^{V}O_4^- + H_2O \quad [2]$$

The Mn^{III} reactive site ($Mn^{III}OOH$ in Equations 3 and 4) on the Mn-oxide surface should be less reactive than a Mn^{IV} reactive site, in oxidizing As^{III} (*20*). While much of the As^{V} produced during As^{III} oxidation by phyllomanganates is released into solution, As^{V} is also sorbed on the solid phase which can also cause passivation of the mineral surface (*6*, *20*, *21*). Passivation of phyllomanganates may also result due to the formation of a Mn/As precipitate under certain reaction conditions (*7*).

$$2Mn^{IV}O_2 + H_3As^{III}O_3 + H_2O \rightarrow 2Mn^{III}OOH + H_2As^{V}O_4^- + H^+ \quad [3]$$

$$2Mn^{III}OOH + H_3As^{III}O_3 + 3H^+ \rightarrow 2Mn^{II}(aq) + H_2As^{V}O_4^- + 3H_2O \quad [4]$$

There are four possible pathways for the oxidation of As^{III} by δ-MnO_2. Each pathway employs a different combination of Mn reactive sites on the δ-MnO_2 surface for As^{III} oxidation (*19*). In the first pathway, one As^{III} molecule reacts with one Mn^{IV} reactive site (represented by $>Mn^{IV}$-OH in Equations 5 – 7; protonation states based on Peacock and Sherman (*22*)) producing one As^{V} molecule and one

In Advances in the Environmental Biogeochemistry of Manganese Oxides; Sparks, et al.;
ACS Symposium Series; American Chemical Society: Washington, DC, 2015.

Mn^{II} molecule (Equation 5). One As^{III} molecule could also react with two Mn^{IV} reactive sites producing one As^{V} molecule and two Mn^{III} reactive sites (represented by $>Mn^{III}\text{-}OH_2$ in Equations 6 - 8; protonation state based on Ramstedt et al.) (Equation 6) (*23*).

$$>Mn^{IV}\text{-}OH + H_3As^{III}O_3(aq) \rightarrow Mn^{II}(aq) + HAs^{V}O_4^{2-}(aq) + 3H^+ \quad [5]$$

$$2(>Mn^{IV}\text{-}OH) + H_3As^{III}O_3(aq) + H_2O \rightarrow 2(>Mn^{III}\text{-}OH_2) + HAs^{V}O_4^{2-}(aq) + 2H^+ \quad [6]$$

The third and fourth possible As^{III} oxidation pathways necessitate that the $\delta\text{-}MnO_2$ surface first contain Mn^{III} reactive sites. One proposed mechanism for Mn^{III} formation is directly through As^{III} oxidation (Equations 3 and 6) (*16*). Some recent studies show that Mn^{III} can form by conproportionation of Mn^{II} and Mn^{IV} at the $\delta\text{-}MnO_2$ surface. In this reaction, Mn^{II} is oxidized, Mn^{IV} is reduced, and the resulting product is Mn^{III} (*24*, *25*). Mn^{III} resulting from conproportionation of Mn^{II} and Mn^{IV} could produce soluble Mn^{III}, however, if there is no ligand to stabilize Mn^{III} in the reactions discussed here, soluble Mn^{III} should rapidly disproportionate back into Mn^{II} and Mn^{IV} (*26*). Thus one can assume that all Mn^{III} in these reactions is associated with the $\delta\text{-}MnO_2$ surface.

One possibility for As^{III} to be oxidized by Mn^{III} is via the reaction of one As^{III} molecule with one Mn^{III} reactive site and one Mn^{IV} reactive site, resulting in one As^{V} molecule, one Mn^{II} molecule and one Mn^{III} reactive site (Equation 7). The other possible pathway for As^{III} oxidation by $\delta\text{-}MnO_2$ is for one As^{III} molecule to react with two Mn^{III} reactive sites creating one As^{V} molecule and two Mn^{II} molecules (Equation 8) (*15*, *19*).

$$>Mn^{IV}\text{-}OH + >Mn^{III}\text{-}OH_2 + H_3As^{III}O_3(aq) \rightarrow Mn^{II}(aq) + >Mn^{III}OH_2 + HAs^{V}O_4^{2}(aq) + 3H^+ \quad [7]$$

$$2(>Mn^{III}\text{-}OH_2) + H_3As^{III}O_3(aq) \rightarrow 2Mn^{II}(aq) + HAs^{V}O_4^{2-}(aq) + H_2O + 4H^+ \quad [8]$$

Advances in Time-Resolved Molecular Scale Techniques To Elucidate Reactions at the Mineral/Water Interface

In soil environments, chemical reactions at the mineral/water interface occur over a range of time scales, from microseconds to years. Many important processes (e.g., adsorption, oxidation-reduction, precipitation) at mineral surfaces are characterized by a rapid, initial reaction that occurs from milliseconds to minutes (*13*, *27–31*). In fact, in some reaction processes, a large part of the reaction process is complete before the first experimental measurement can be made using traditional batch and flow techniques. An understanding of these initial reaction rates, where back reactions and secondary reaction products are minimized, allows one to obtain "chemical kinetic" rate constants and reaction mechanisms, both of which are needed to understand environmental chemical processes. Chemical relaxation techniques e.g., pressure jump (p-jump) and concentration jump (c-jump such as stopped-flow), provide rapid data collection on time scales of milliseconds. However, with these methods, rate “constants” are calculated from linearized rate equations that include parameters that were

In Advances in the Environmental Biogeochemistry of Manganese Oxides; Sparks, et al.;
ACS Symposium Series; American Chemical Society: Washington, DC, 2015.

determined via macroscopic equilibrium and modeling studies. Thus, the rate "constants" are not directly determined (*13*, *32*, *33*).

Direct, in situ, molecular-scale measurement of rapid reactions has been limited. Fendorf et al. (*34*) employed stop-flow electron paramagnetic resonance (SF-EPR) spectroscopy to determine Mn(II) sorption on birnessite (δ-MnO_2) at a time scale of milliseconds. Recently, Parikh et al. (*14*) used in situ, Fourier Transform infrared (FTIR) spectroscopy to determine As(III) oxidation rates on hydrous manganese(IV) oxide (HMO) at a time resolution of ~2.5 s. Unfortunately, both of these techniques have limitations. EPR can only be used to measure EPR active nuclei, while FTIR requires both IR active functional groups and relatively high concentrations of reactants (*14*).

These are not limitations with quick-scanning X-ray absorption spectroscopy (Q-XAS). Q-XAS is a synchrotron-based technique that allows one to collect a X-ray absorption near edge structure (XANES) or extended X-ray absorption fine structure (EXAFS) spectrum on ms time scales (*35*).

Depending on beamline instrumentation and photon flux, Q-XAS, can probe elements with atomic numbers >20 and at low concentrations (*36*). Most of the quick-scanning beamlines allow for collection of a complete EXAFS scan in ~ 1 min or less, by slewing the monochromator from low energy to high energy and repeating the process (*37*). Another way to rapidly collect EXAFS data is to conduct energy-dispersive measurements; however, this technique often has poor sensitivity and since transmission mode is used, it may be unsuitable for mineral/ water studies (*35*).

Ginder-Vogel et al. (*13*), for the first time, employed Q-XAS to measure the kinetics of As(III) oxidation on hydrous manganese oxide (HMO). A cam-operated, continuously scanning monochromator (Figure 1) was used at beamline X18B at the National Synchrotron Light Source (NSLS) at Brookhaven National Laboratory. The constant rocking motion enabled the collection of X-ray fluorescence spectra as the monochromator moved from low to high and from high to low energy. This enabled greater time resolution of the XAS measurements.

Q-XAS has been employed over the past several years to study metal sorption/ precipitation (*31*) and redox kinetics (*13*, *30*) using both batch and flow apparatus.

Kinetics and Mechanisms of As(III) Oxidation on Mn-Oxides

While the mobility and toxicity of elements such as As and Cr is dependent on redox state and the redox conditions of the environment, the kinetics of the processes also play an important role. XAS is an ideal tool for determining the local coordination environment of an element and its oxidation state and for following changes in speciation and reaction mechanisms over time (*38*).

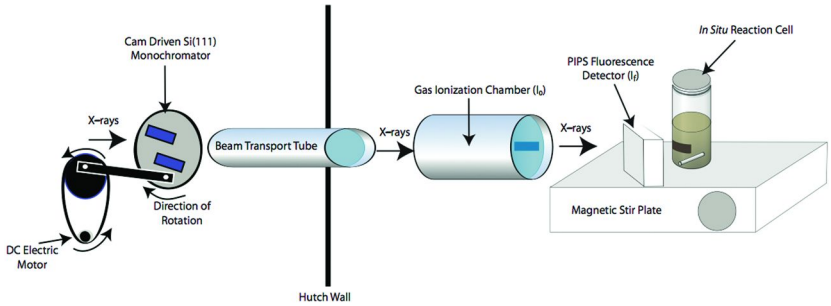

Figure 1. Experimental setup used to collect Q-XAS data. Reproduced with permission from Ginder-Vogel et al. PNAS 106, 16124–16128. Copyright (2009) National Academy of Sciences.

Parikh et al. (*39*), using single bounce, rapid scan attenuated total reflectance Fourier transform infrared (ATR-FTIR) spectroscopy, demonstrated that As(III) oxidation on HMO was extremely rapid. In the research of Ginder-Vogel et al. (*13*), using Q-XAS, a complete XANES spectrum was collected in 980 ms (Figure 2). In this study the oxidation states in both the solution and at the mineral/water interface were probed. The average oxidation state was then determined by fitting each individual XANES spectra with a linear combination of As(III) and As(V) standard solutions (in this experiment, 5 mM standards were used). The fits yielded the molar ratio of As in solution, from which the concentrations of As(III) and As(V) could be calculated, using the initial As concentration. In Figure 3 one sees the XANES spectra for the reaction of As(III) with HMO over time scales ranging from 0.98 to 298.9 sec. There is a rapid transformation of As(III) to As(V) on the HMO surface. Complementary solution and surface concentrations for both Q-XAS and separate batch experiments show that after 1 sec, the As(V) concentration reaches 0.37 mM (Figure 3) and increases precipitously for 45 sec to attain a concentration of 1 mM, and then slowly reaches 1.5 mM after 300s. Based on biphasic kinetics, rate constants were determined from first-order plots for both the Q-XAS and batch experiments (Table 1). For both methods, a rate constant for As(III) depletion was obtained that was an order of magnitude larger during the initial portion of the reaction that in the later segment (Table 1). The initial rate constant of As(III) depletion, obtained using Q-XAS was nearly twice as large (4.7×10^{-3} /sec) as the rate constant determined with the batch method (2.5×10^{-3}/sec, Table 1).

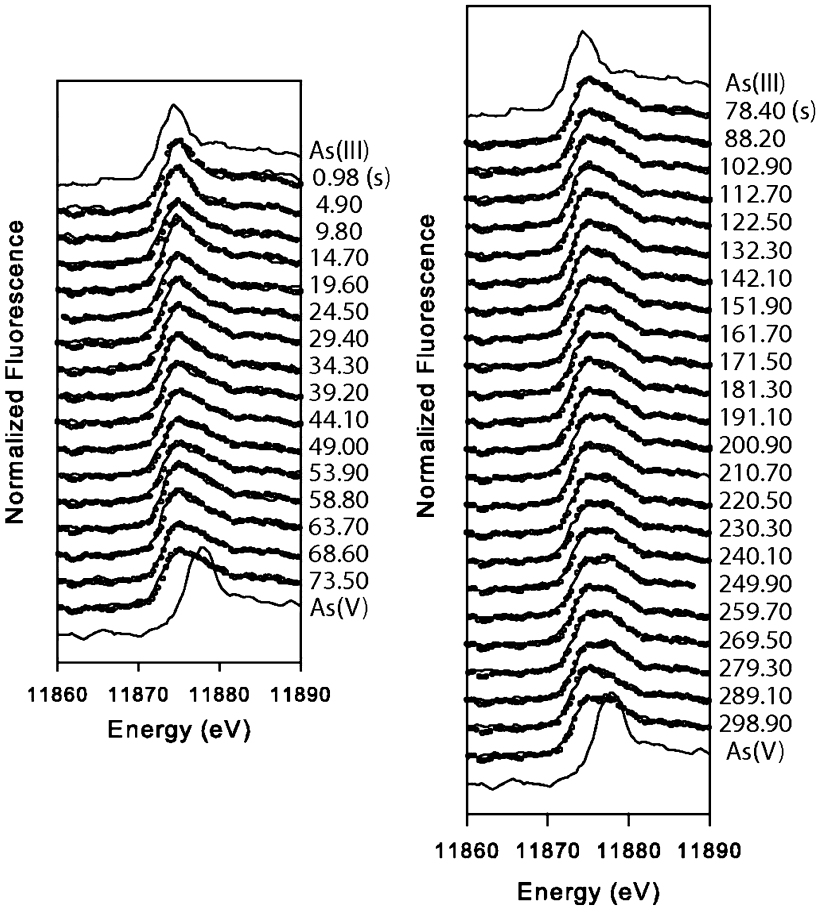

Figure 2. Data (solid) and linear combination fits (dots) of individual As K-edge XANES spectra used to determine As(III) and As(V) concentrations during the batch reactions. Each spectrum was collected in approximately 980 ms, with the time (in s) next to each spectrum indicating the time the last data point of each spectrum was collected. Reproduced with permission from Ginder-Vogel et al. PNAS 106, 16124–16128. Copyright (2009) National Academy of Sciences.

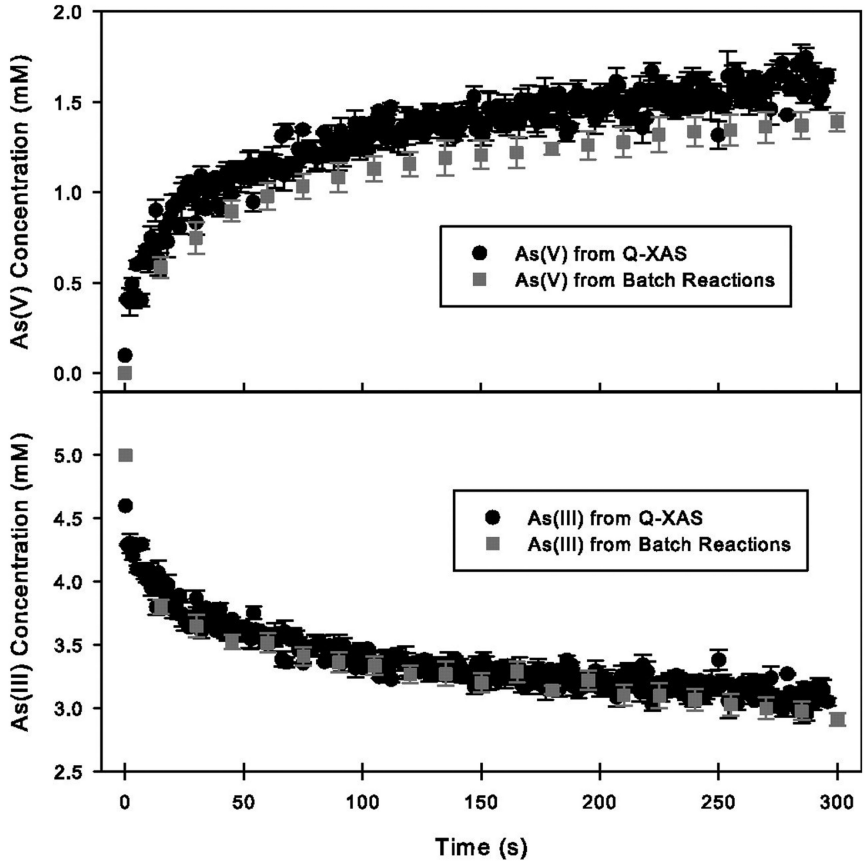

Figure 3. As(V) and As(III) concentrations determined from traditional batch and Q-XAS reactions. Error bars represent the SD of 3 measurements made at each time point. XANES spectra and fits used to calculate Q-XAS As concentrations are shown in Figure 12. Reproduced with permission from Ginder-Vogel et al. PNAS 106, 16124–16128. Copyright (2009) National Academy of Sciences.

Table 1. Apparent, first-order rate constants determined from batch and Q-XAS experiments[a]

Experiment type	*Time period (s)*	*No. of data points*	*k* (s^{-1})	r^2
As(III)–Batch	1–60	4	2.5 (3) × 10^{-3}	0.96
As(III)–Batch	135–300	14	6.1 (4) × 10^{-4}	0.82
As(III)–Q-XAS	1–30	30	4.7 (4) × 10^{-3}	0.91
As(III)–Q-XAS	135–300	168	4.9 (4) × 10^{-4}	0.74

[a] The rate constants of As(III) depletion were determined by linear regression analysis of the noted time-periods.vReproduced with permission from Landrot et al. Environ. Sci. Technol. *44*, 143–149. Copyright (2010) American Chemical Society.

Lafferty et al. (*15*, *40*), using a combined kinetic and molecular scale approach, determined the rates and mechanisms of As(III) oxidation and As desorption on hydrous manganese oxide (HMO), a high surface area, amorphous Mn-oxide. A stirred-flow technique was employed to follow the kinetics of As(III) oxidation over a time scale of days (Figure 4). During the first 0.4 hour no As or Mn appeared in the effluent solutions, indicating that all the As(III) was oxidized to As(V) since the EXAFS data did not show any sorption of As(III) on the HMO. Up until 6.4 hours, only As(V) appeared in the effluent solution suggesting that all the As(III) was oxidized to As(V) and bound to the HMO or was desorbed into the solution phase. After 6.4 hours, As(V), as well as Mn(II) and As(III), appeared in the effluent. This was also when As(III) oxidation decreased. Synchrotron-based XRD and XAS analyses of Mn revealed that initially Mn was sorbed into vacancy sites of the HMO as both Mn^{2+} and Mn^{3+}, and at between 4 and 10 hours the vacancy sites were filled and Mn^{2+} began to compete with As(V) for edge sites, causing a decrease in As(IIII) oxidation. Additionally, the data indicated that Mn^{3+} could be sorbing on edge sites via conproportionation. This results when Mn^{2+} is oxidized and Mn^{4+} is reduced. Thus, passivation of the HMO surface was significantly affected not only by As(V) but most importantly, Mn^{2+} and Mn^{3+}. As time proceeded, passivation of the surface was enhanced. XAS of As speciation showed that only As(V) species were present on the surface, but that the type of As(V) species changed as reaction time proceeded (Figure 5). Up to 4 hours of reaction time, the predominant inner-sphere adsorption complexes were bidentate binuclear and monodentate mononuclear but between 4 and 10 hours, when passivation ensued, there were two predominant species, bidentate binuclear and a bidentate mononuclear. A schematic showing the overall mechanism of As(III) oxidation on HMO is shown in Figure 6. The data clearly show, once again, the importance of following reaction processes over time and at the molecular scale.

Effect of Competitive Ions and Bacteria on As(III) Oxidation on Mn-Oxides

Some studies have been published on the competitive effects of elements and bacteria on the kinetics of As(III) oxidation on Mn-oxides (*41*, *42*). Ion competition does impact As(V) sorption on minerals (*41*, *43–45*), but few studies have appeared on the effect of ion competition on As(III) oxidation kinetics on Mn-oxides (*8*, *41*). Chiu and Hering (*9*) showed that reactions with manganite were slower than what was observed for As(III) oxidation on poorly crystalline Mn(IV) oxides (*13*, *39*). Parikh et al. (*41*) studied the effects of Fe and phosphate competition on the rapid, initial kinetics of As(III) oxidation on δ-Mn-oxide. Phosphate caused decreased total As sorption on Mn-oxide (Figure 7). This could be ascribed to the similar chemical structure and reactivity of As(V) and phosphate (*41*, *44*, *46*). There was also decreased retention of both anions (Figure 7). The reduced As sorption in the presence of phosphate is advantageous in environments where animal waste containing both As and P is land applied (*41*).

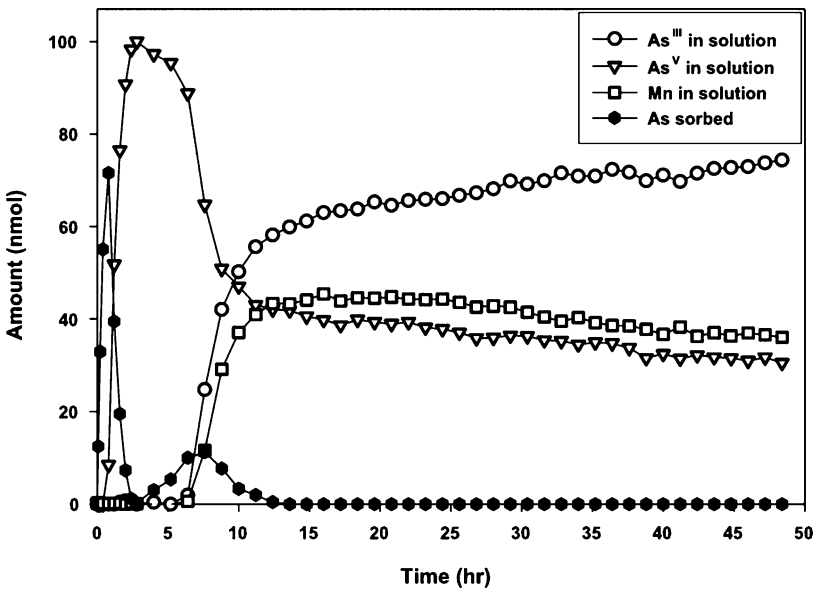

Figure 4. The amount (nmol) of As sorbed as well as amounts (nmol) of AsIII, AsV, and MnII in the effluent of a stirred-flow experiment reacting 1 g/L δ-MnO2 with 100 μM AsIII flowing at 1 mL/min for 48 h. Reproduced with permission from Lafferty et al., Environ. Sci. Technol. 44, 8460-8466. Copyright (2010) American Chemical Society.

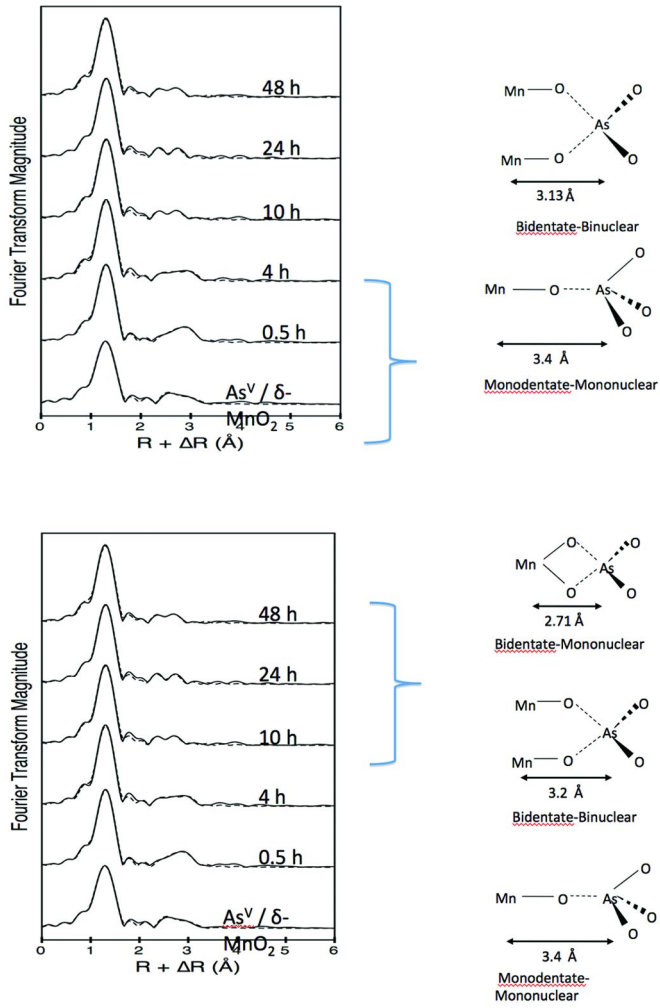

Figure 5. Time 0 through 4 h AsV is bound in Bidentate-Binuclear and Monodenate-Mononuclear. This is the time when Mn is primarily sorbing at vacancy sites. Time 10 through 48 h AsV is bound in Bidentate-Binuclear, Monodenate-Mononuclear, and Bidentate-Mononuclear. Bidentate-binuclear As-Mn length increases. Mn(III) is present when AsV bonding changes. This is the time when Mn has filled all vacancy sites and begins to compete with As for edge sites. Reproduced with permission from Lafferty et al., Environ. Sci. Technol. 44, 8467–8472. Copyright (2010) American Chemical Society.

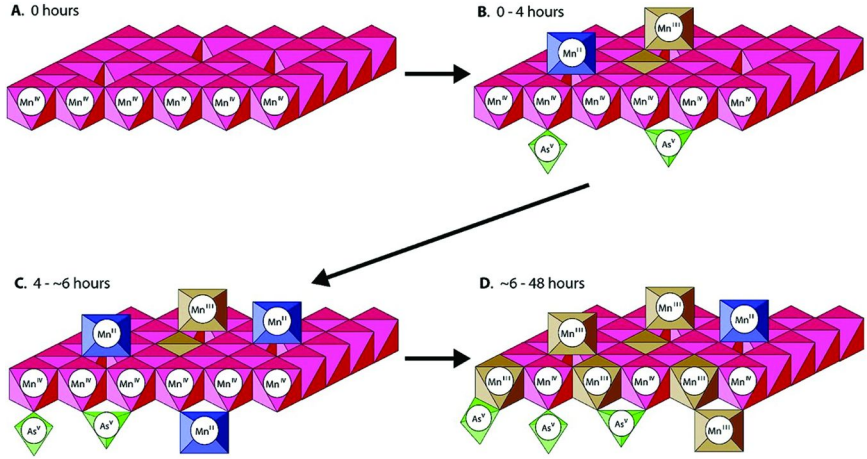

Figure 6. Proposed reaction mechanism for AsIII oxidation by δ-MnO2 over 48 h in a stirred-flow reactor. Throughout the reaction, AsIII is oxidized by MnIV at δ-MnO2 edge sites, producing MnII and AsV. (A) Unreacted δ-MnO2 octahedral layers consist of primarily Mn4+ and have reaction sites at layer edges (edge sites) and vacancy sites. (B) During the first 4 h of AsIII oxidation, MnII sorbs at δ-MnO2 vacancy sites, and AsV sorbs at edge sites in bidentate−binuclear and monodentate−mononuclear complexes. Also, a portion of sorbed MnIIreacts with MnIV at vacancy sites to form MnIII. (C) Between 4 and 6 h of reaction, vacancy sites become filled with MnII/III, MnII begins to sorb at δ-MnO2 edge sites, and AsV sorption continues in the same sorption complexes. (D) Beyond 6 h of reaction, MnII at edge sites (and probably vacancy sites) reacts with MnIII in δ-MnO2 octahedral layers to form MnIII. The resulting MnIII changes the bonding environment of AsV, which begins to sorb in bidentate−mononuclear complexes, and the As−Mn distance in AsV bidentate−binuclear complexes increases slightly. Reproduced with permission from Lafferty et al., Environ. Sci. Technol. 44, 8467–8472. Copyright (2010) American Chemical Society.

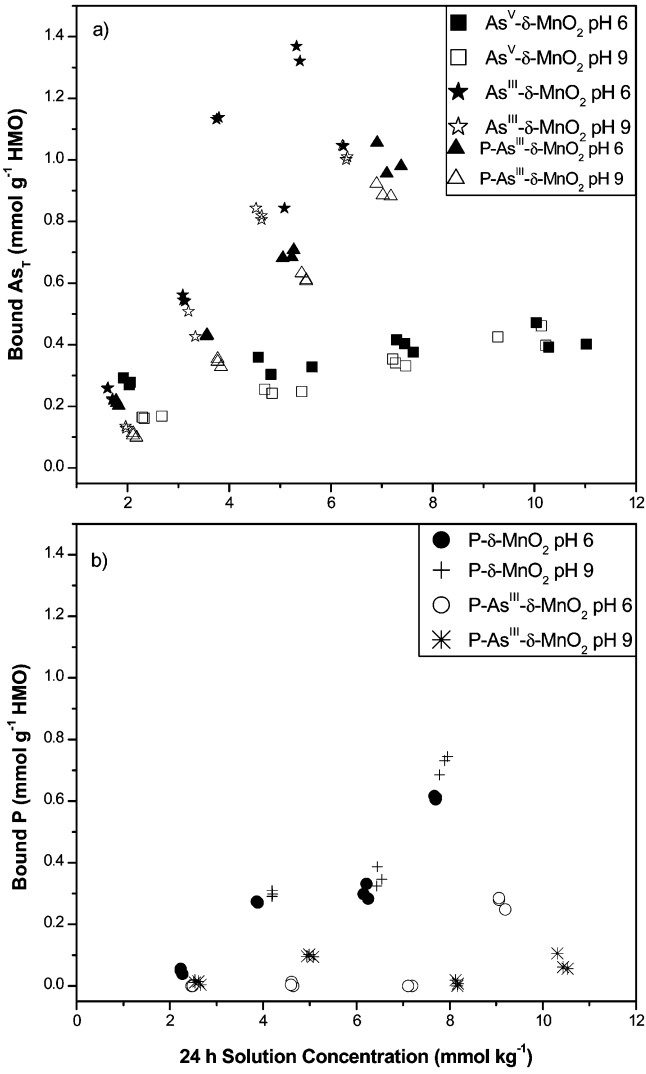

Figure 7. Sorption isotherms from batch experiments at pH 6 (solid symbols) and 9 (open symbols) in 5 mmol kg−1 NaCl for a) As sorption to δ-MnO2 when added as AsV and AsIII (including oxidation) in the presence and absence of phosphate (P) and b) phosphate sorption to δ-MnO2 in the presence and absence of AsIII. Reproduced with permission from Parikh et al., Environ. Sci. Technol. 44, 3772-377. Copyright (2010) American Chemical Society.

Figure 8 shows the percent of initial As [As(III) and As(V)] and phosphate in solution after reaction with Mn-oxide over time at pH 6 and 9. An increased rate of As(III) oxidation on manganite was previously observed with decreased pH (6.3 to 4); however, the current data, and the study of Parikh et al. (*14*) showed no significant effect of pH on the initial As(III) oxidation on Mn-oxide (Figure 8). The concentration of As(III) in solution rapidly dropped to near zero, with full removal from solution occurring between 5 and 30 minutes. At 24 h, both phosphate and As concentrations were stable, with solution As(V) concentrations higher when phosphate was present. When the As(V) concentrations were increased from 5 to 960 minutes reactions are still occurring at the solid-liquid interface. There were still high phosphate concentrations in solution, which indicated that As release was not due to phosphate exchange reactions (*41*).

Figure 9 shows the effect of phosphate and γ-Fe-oxide on As(III) oxidation on Mn-oxides using rapid scan ATR-FTIR. In every case the addition of phosphate reduced the total amount of As(III) oxidation. The initial slope and half times were similar for all reactions, except for the addition of 25 mmol kg-1 phosphate (the slope decreased and half time increased). Although phosphate and α-FeOOH concentrations reduced the amount of As(V) produced, the initial oxidation rate was not affected. Since the initial reaction rates were not strongly influenced by concentration of reactants, including other ions and surfaces, the reaction did not appear to be transport limited, which suggests that primarily chemically controlled kinetics were measured (*41*).

Under certain conditions, As(III) can be oxidized by Fe-oxides (*47*) however, no oxidation by α-FeOOH was observed during 15 minutes of reaction (Figure 9). When δ-Mn-oxide was reacted with As(III) and 4 g kg-1 α-FeOOH, the amount of As(V) detected decreased. However, with increasing α-FeOOH concentration the amount of As(V) increased. At the highest α-FeOOH concentration the amount of As(V) produced exceeded what was observed for δ-Mn-oxide alone (Figure 9). The reduced As(III) oxidation in the presence of α-FeOOH is ascribed to competition between δ-Mn-oxide and α-FeOOH for As(III). Increasing α-FeOOH increased competition for As(V), and with high α-FeOOH concentrations, some As(V) released from δ-Mn-oxide during oxidation binded to the α -FeOOH instead of δ-Mn-oxide. Therefore, passivation of δ-Mn-oxide was reduced. In this case, the Fe-oxide was promoting and hindering As(III) oxidation on δ-Mn-oxide. This result was observed when As(III) was oxidized by birnessite, todorokite, and hausmannite in the presence of α-FeOOH (*41*, *48*). Another study showed an increase in As attenuation via simultaneous oxidation of As(III) and Fe(III) by Mn-oxides, whereby coprecipitation of Fe(III)-oxides with As(V) sequestered As and prevented Mn-oxide passivation (*41*, *49*).

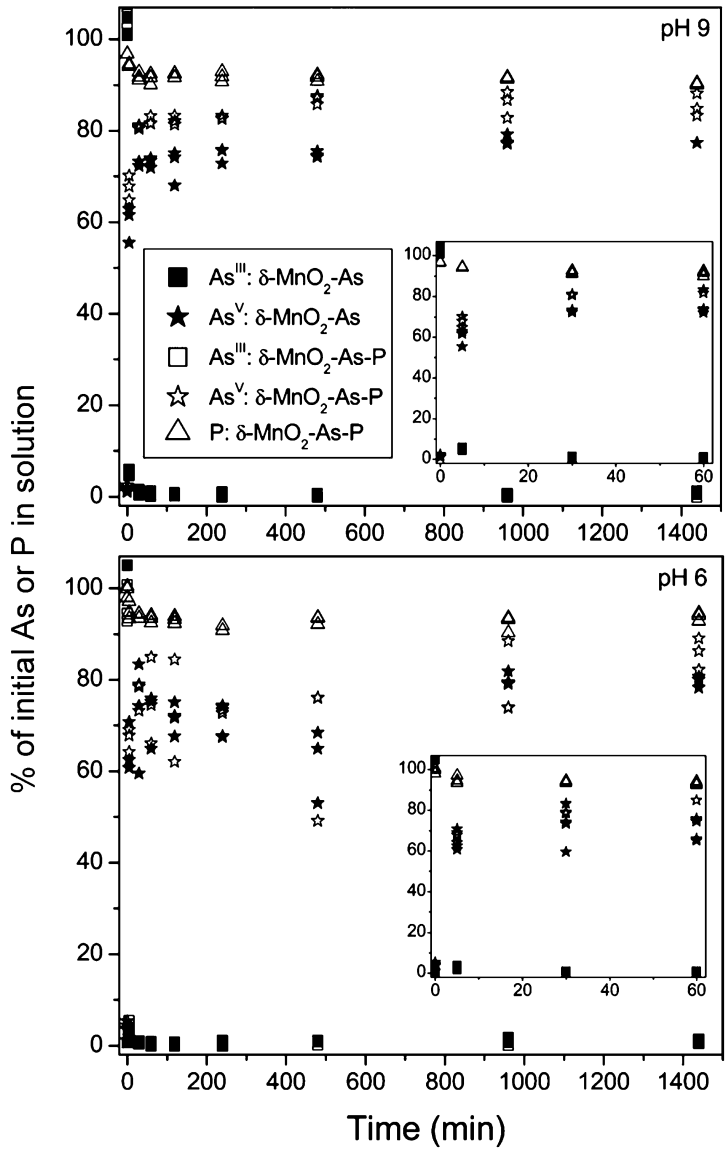

Figure 8. Kinetic plots of batch experiments showing percent of initial As (5 mmol L−1 AsIII), as solution AsIII and AsV, and phosphate in solution during the course of reaction with δ-MnO2 at a) pH 9 and b) pH 6 in 5 mmol kg−1 NaCl. Insets are included to allow viewing of data within the first 60 min of reaction. Solid symbols correspond to experiments where δ-MnO2 was reacted with AsIII, and open symbols correspond to experiments where AsIII and phosphate were simultaneously reacted with δ-MnO2. Reproduced with permission from Parikh et al., Environ. Sci. Technol. 44, 3772-377. Copyright (2010) American Chemical Society.

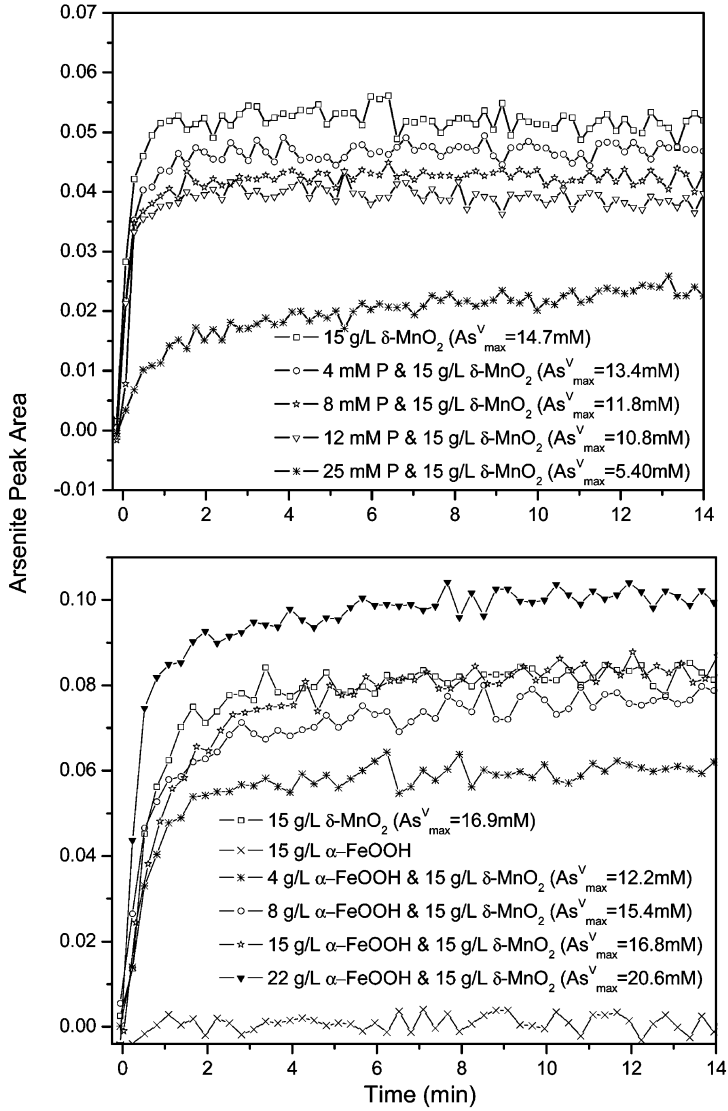

Figure 9. Rapid-scan ATR-FTIR plots of AsV IR peak area as a function of reaction time for 25 mmol kg−1 AsIII (pH 6, 5 mmol kg−1 NaCl) reacted with varying concentrations of a) phosphate (P) and b) α-FeOOH (experiments conducted on a different FTIR and with different batches of δ-MnO2 and α-FeOOH). Reproduced with permission from Parikh et al., Environ. Sci. Technol. 44, 3772-377. Copyright (2010) American Chemical Society.

Parikh et al. (*41*) also studied the effect of bacteria on As(III) oxidation on Mn-oxide. Solution As(III) and As(V) concentrations, over a 48 hour reaction period, showed that the bacteria completely oxidized 1 mmol kg-1 As(III) in about 24 hours. The data also showed that the bacteria oxidize a maximum of about 5 mmol kg-1 As(III) in 48 hours, with the highest oxidation rate occuring after 24 hours of reaction. Rapid-scan ATR-FTIR experiments did not show detectable As(III) oxidation by either *P. fluorescens* or *A. faecalis* alone during the 15 min reaction time (Figure 10) and rapid As(III) oxidation was observed only when Mn-oxide was present. When bacteria were bound to only α-FeOOH, no As(V) was detected; however, if δ-Mn-oxide was present with bacteria, a small IR peak corresponding to As(V) was observed.

The As(V) max for *P. fluorescens* with Mn-oxide was 3.05 mmol kg-1 and 4.41 mmol kg-1 for *A. faecalis* with Mn-oxide; with α-FeOOH also present the values dropped to 0.79 and 2.14, respectively. The half-time values were less than when δ-Mn-oxide reacted with As(III) alone, with values ranging from 0.64 to 0.88; however, the slope values were much less with a value of 0.01. Bacterial adhesion to minerals blocks access to Mn(IV) and reduces the As(V) maximum. Bacteria bound to δ-Mn-oxide impede As(V) production much more than reaction with phosphate or α-FeOOH. Reaction rates were significantly reduced, based on half-times (0.9802.81) and m30 s (0.01) values, which suggest that the reaction was transport limited. Exchange of bacteria or biopolymers for As(III) at Mn(IV) sites was not likely. Rather, the As(III) diffusion and transport through bacteria extracellular material (biofilm) proabley retarded As(III) oxidation (*41*).

Jones et al. (*42*) studied the kinetics of As(III) oxidation by two heterotrophic soil bacteria (*Agrobacterium tumefaciens* and *Pseudomonas fluorescens*) and poorly crystalline manganese oxide (δ-Mn-oxide) using batch experiments. The apparent rate of As(V) appearance in solution was higher for the combined batch experiments in which bacteria and δ-Mn-oxide were oxidizing As(III) at the same time than for either component alone. The additive effect of the mixed bacteria and δ-Mn-oxide system was consistent for short (<1 h) and long (24 h) term coincubation showing that mineral surface inhibition by cells had little effect on the As(IIII) oxidation rate. Surface interactions between cells and the mineral surface were indicated by sorption and pH-induced desorption data. Total sorption of As on the mineral was lower with bacteria present (16.1 t- 0.8% As sorbed) and higher with δ-Mn-oxide alone (23.4+- 1%). Arsenic was more easily desorbed from the cell- δ-Mn-oxide system than from δ-Mn-oxide alone. Therefore, the presence of bacteria inhibited As sorption and decreased the stability of sorbed As on δ-Mn-oxide even though As(III) was oxidized most rapidly in a mixed cell- (δ-Mn-oxide system. The additive effect of biotic (As-oxidizing bacteria) and abiotic (δ-Mn-oxide mineral) oxidation processes in a system containing both oxidants suggests that mineral-only data may underestimate the oxidative capacity of natural systems with biotic and abiotic As(III) oxidation pathways (*42*).

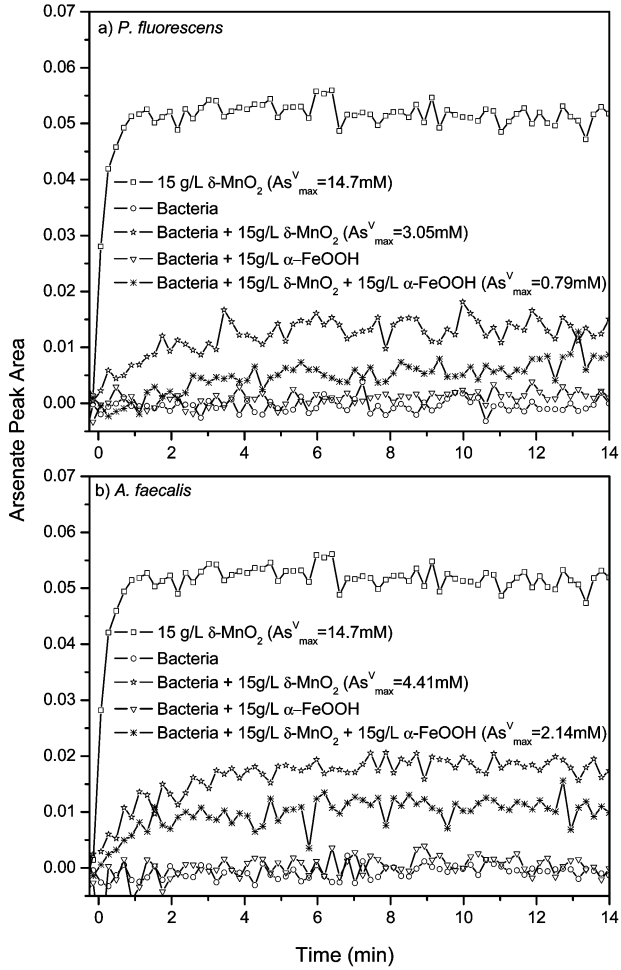

Figure 10. Rapid-scan ATR-FTIR plots of AsV IR peak area as a function of reaction time for 25 mmol kg−1 AsIII (pH 6, 5 mmol kg−1 NaCl) reacted with a) P. fluorescens and b) A. faecalis suspensions (10 times steady state) with and without δ-MnO2 and α-FeOOH. Reproduced with permission from Parikh et al., Environ. Sci. Technol. 44, 3772-377. Copyright (2010) American Chemical Society.

Environmental Influences on Cr(III) Oxidation on Mn-Oxides

Chromium predominantly exists in two oxidation states in the environment, Cr^{III} and Cr^{VI} (*50*, *51*). Chromate, chromium(VI), is highly toxic to animals and plants; moreover, it is quite soluble and highly mobile under environmental conditions. The other common Cr oxidation state, chromite (Cr^{III}), is less toxic and generally immobile. Most Cr in the environment is present as Cr^{III}; however, industrial processes and Mn-oxides can oxidize Cr^{III} into Cr^{VI} and release this toxic metal into natural systems (*52*, *53*). The widespread contamination of natural systems with Cr^{VI} necessitates a thorough understanding of the mechanisms of Cr oxidation by Mn-oxides to determine the risk of Cr^{VI} production and develop techniques to reduce its formation.

Mn-oxides are the only naturally occurring mineral capable of oxidizing Cr^{III} (*52*, *53*). While all Mn-oxides are able to oxidize Cr, the extent and rate of Cr^{VI} production is highly dependent on the mineral's surface charge, PZC, surface area, Mn^{II} and Mn^{III} impurities, and the reactive site density of Mn^{IV} (*54*). Most naturally occurring Mn-oxides are poorly crystalline with layered structures. Random stacked birnessite (RSB), acid birnessite (AB), and δ-MnO, are synthesized Mn-oxides which closely resemble those found in the environment. All of these Mn-oxides can rapidly convert a large percentage of Cr^{III}, up to 80%, into Cr^{VI} (*55–57*). Many other Mn-oxides, such as birnessite, manganate, hausmanite, and Mn_2O_3 can also quickly oxidize Cr^{III} (*57*, *58*). Even pyrolusite, which has the highest PZC and is the most crystalline of the Mn-oxides, can oxidize Cr^{III} to Cr^{VI} in small quantities (*53*, *57*).

The oxidative capacity of Mn-oxides can be quantified through the use of batch techniques. Kim *et al.* (*58*) and Weaver & Hochella (*57*) determined this capacity under relatively similar experimental conditions. Weaver & Hochella (*57*) found birnessite had the highest oxidizing ability followed by hausmannite, romanechite, cryptomelane, manganite, pyrolusite, and lithiophorite, in order of decreasing reactivity. Kim *et al.* (*58*) found birnessite to be the most reactive, followed by todorokite, lithiophorite, and finally pyrolusite. The reactivity of Mn-oxides can be closely linked to their degree of crystallinity, which influences surface area (*57–59*). Birnessite has the largest surface area and is the most reactive; however, the relationship between oxidative capacity and surface area is broken by hausmannite, which has a smaller surface area than romanechite and cryptomelane. Excluding hausmannite, surface area is a strong predictor of Cr^{III} oxidation. Kim & Moon's (*59*) study reinforces this trend, showing up to a 20% increase in Cr^{VI} production by a less crystalline birnessite. Biogenic manganese oxides (bioMnOx) follow a similar pattern, where younger, less structured bioMnOx have greater reactivity compared to more aged bioMnOx that contain higher proportions of triclinic birnessite (*60*). The percentage of Cr^{III} oxidation by Mn-oxides is also dependent on the oxidation state of Mn on the mineral surface (*59*), where a higher Mn^{IV} concentration leads to larger amounts of Cr^{III} oxidized. This is due to Cr^{III} supplying two electrons to Mn^{IV} versus only one to Mn^{III} (*58*).

The Cr oxidation reaction proceeds in three phases, first Cr sorbs to the Mn surface, then the Cr exchanges electrons with Mn, and finally the reaction products

In Advances in the Environmental Biogeochemistry of Manganese Oxides; Sparks, et al.;
ACS Symposium Series; American Chemical Society: Washington, DC, 2015.

are desorbed (*52*, *56*, *61*, *62*). The exact kinetics and mechanisms of Mn-oxidation are poorly understood (*63*). An overall equation for the oxidation of Cr(III) is shown in Eq. 9 and a schematic of the multimodal processes is shown in Fig. 11 (*64*).

$$Cr(OH)^{2+} + 1.5MnO_2 \leftrightarrow HCrO_4^- + 1.5Mn^{2+} \quad [9]$$

The pH of the solution can greatly impact Cr oxidation kinetics. As pH rises, the Mn mineral surface becomes more negative, further attracting positively charged Cr^{III}. This increases the electrostatic interaction between the Mn mineral surface and Cr^{III}. Accordingly, more Cr^{III} is sorbed to the Mn surface leading to initially higher rates of Cr^{VI} production (*65*). However, not all of the Cr^{III} is oxidized because Mn^{IV} and Cr^{III} share the same structural environment. Therefore, some of the Cr^{III} can be sorbed to the surface of the manganese and remain un-oxidized. Cr^{III} sorption preferentially occurs at higher pHs, allowing Cr^{III} to be held as an inner-sphere complex on the $Mn(IV)O_2$ surface. This contrasts with Cr^{VI} which is thought to form primarily outer-sphere complexes with Mn-oxide (Fig. 11). Higher pHs ultimately lower the amount of Cr^{III} oxidized which reduces the production of Cr^{VI} (*66*).

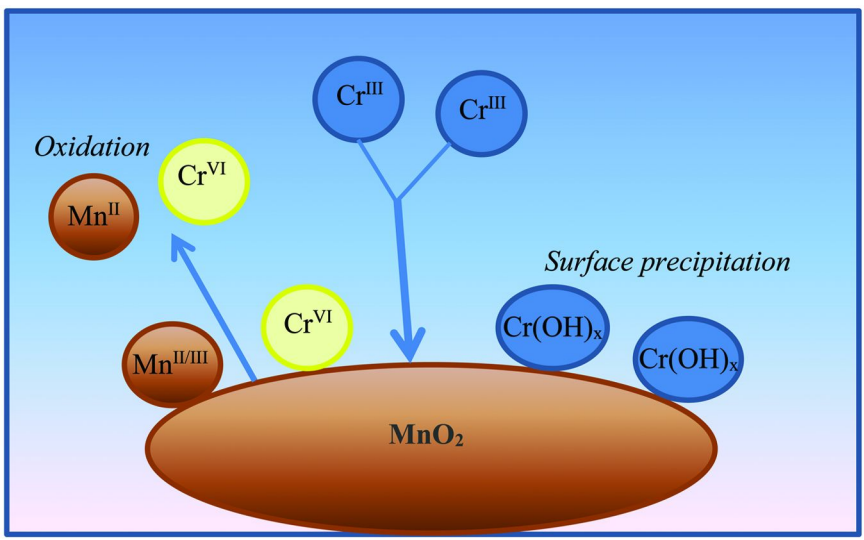

Figure 11. The Cr^{III} in solution interacts with the surface of MnOx. Some of the Cr^{III} is sorbed to the surface of the MnOx, while some is oxidized. Not all of the Cr^{VI} is released back into solution as a portion can sorb on the MnOx surface.

Research conducted by Johnson & Xyla (*61*) determined a lower rate of Cr^{III} oxidation by manganite as Cr^{III} concentrations increased. Fendorf and Zasoski also found Cr^{III} oxidation by birnessite was reduced at higher Cr^{III} concentrations (*65*). In both cases, Cr^{III} was below a pH and concentration where it could precipitate in solution alone. Similarly, as the solution pH increases more hydroxide ions are introduced into the reaction, enhancing the formation of Cr hydroxide precipitates on the Mn mineral surface. Fendorf & Zasoski (*65*) determined there was little change in reactivity from pH 2 to 3.5. However, above pH 3.5, the increased availability of hydroxide ions enhanced the formation of Cr hydroxides leading to passivation of the Mn mineral surface (*65*). When the pH was raised above 3.5 Cr^{III} oxidation decreased (*66*). This was confirmed by Feng *et al.* (*67*), who found the amount of Cr^{III} oxidized by birnessite between pH 2 and 3.5 was nearly constant, but oxidation of Cr^{III} was reduced once the pH increased beyond 3.5. Experiments conducted by Landrot *et al.* (*66*) showed greater oxidative capacities at more acidic pHs, even within the pH 2.5 to 3.5 range as can be seen in Fig. 12. The combination of higher pHs and concentrations promote the precipitation of Cr-(oxyhdr)oxide phases. The formation of Cr hydroxides on the Mn mineral surface reduces the availability of reactive sites, which in turn decreases Cr^{III} sorption and oxidation. Chromium hydroxide can precipitate from bulk solution onto the surface of Mn minerals at concentrations below its saturation index (*64*).

Under more neutral pH conditions bioMnOx oxidized more Cr^{III} at higher, rather than lower pHs. At pH 6.2 Cr oxidation by bioMnOx ceased within 10 mins, while at pH 7.2 oxidation continued for 160 mins. The quenching of the reaction at pH 6.2 is due to either the proton promoted dissolution of bioMnOx or the lower activity of bioMnOx towards Mn^{II} oxidation (*60*).

Kinetics and Mechanisms of Cr(III) Oxidation on Mn-Oxides

The identification and quantification of chromium oxidation states using XANES spectroscopy is quite straightforward due to a prominent pre-edge peak at 5993 eV, when Cr is present as Cr^{VI} which is caused by a bound-state 1s to 3d transition. Landrot et al. (*29*) employed the same technique as Ginder-Vogel et al. (*13*) to measure the rapid, initial kinetics of Cr^{III} oxidation on HMO (*29*, *49*, *50*). A complete XANES spectrum was determined in 0.75 sec. Data were collected at pHs of 2.5, 3.0, and 3.5 at Cr^{III} concentrations of 40-100 mM. Chromium^{VI} resulting from the oxidation of Cr^{III} on the HMO surface, displays the prominent pre-edge feature in the XAS spectrum, which is proportional to the amount of Cr^{VI} in the system. Therefore, the height of the pre-edge feature can be measured and compared to a set of Cr^{III}/Cr^{VI} mixtures to determine the amount of Cr^{VI} present over the course of the reaction (*29*, *50*). Figure 13 shows the pre-edge feature increases in intensity with time, indicating the oxidation of Cr^{III} to Cr^{VI}. Chromite oxidation is quite rapid during the first 120 sec of the reaction, when about 35 mM of chromate is produced. The reaction continued to oxidize Cr^{III} to Cr^{VI} for another 30 minutes, before oxidation ceased between 30-60 minutes due to sorption of chromate. Initial reaction rates were determined by quantifying

In Advances in the Environmental Biogeochemistry of Manganese Oxides; Sparks, et al.;
ACS Symposium Series; American Chemical Society: Washington, DC, 2015.

the Cr^{VI} from the height of the pre-edge feature for each experiment, focusing on the reaction from 0-1 minute. Landrot et al. found the rate constants were similar at a given pH and for varying Cr^{III} and HMO concentrations (Table 2) (*29*). Strongly suggesting that the k values are chemical rate constants, as only temperature should impact the magnitude of the k values. Therefore, the use of a method like Q-XAS not only provides valuable information on rapid, initial reaction processes, but also the additional benefit of determining chemical kinetics rate constants. Together these findings provide important insights on reaction mechanisms. Most other techniques cannot significantly reduce or eliminate transport processes. Consequently, the rate parameters that are measured are apparent rate coefficients, and not rate constants. The rapid initial oxidation of Cr(III) by HMO was also confirmed by Dai *et al.* (*68*) who discovered Cr^{VI} levels increased quickly within the first 50 minutes of the reaction and increased slowly before leveling off after 300 minutes, due to the saturation of available surface adsorption sites. Techniques such as Q-XAS and further, more detailed research will unlock the exact kinetics and mechanisms of Cr oxidation by Mn-oxides (*69*).

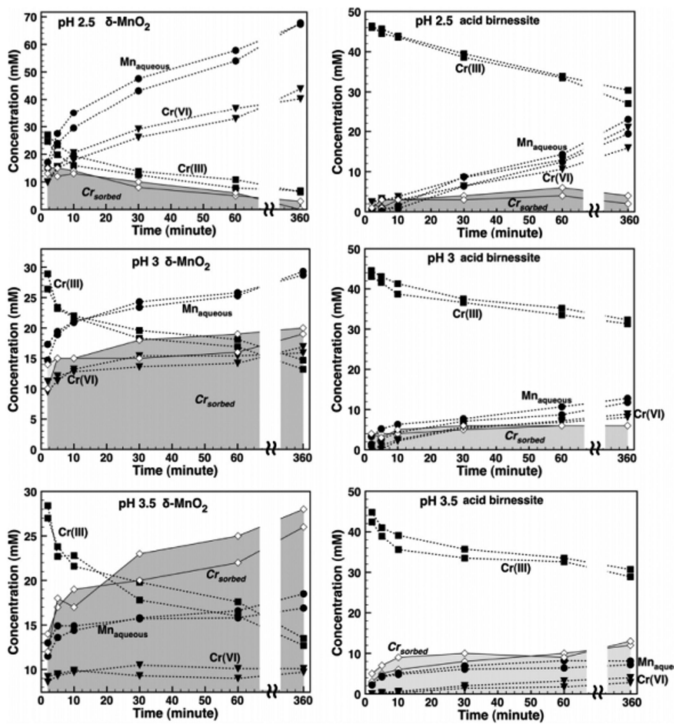

Figure 12. Mn oxides react rapidly with Cr. The reaction is largely complete within the first 20-60 minutes. Lower pHs result in greater oxidation of Cr^{VI}, with less overall surface sorption. Reproduced with permission from Landrot et al., Environ. Sci. Technol. 46, 11594-11600. Copyright (2012) American Chemical Society.

Table 2. Initial Conditions, Measured Initial Rates, and Rate Parameters[a]

		initial rates (mol/L/sec)			k (sec^{-1})		
[Cr(III)] (mM)	[HMO] (g/L)	pH = 2.5	pH = 3	pH = 3.5	pH = 2.5	pH = 3	pH = 3.5
100	20	0.0045/0.0052 *(0.00036/0.00071)*	0.0045/0.0045 *(0.00067/0.00064)*	0.0045/0.0047 *(0.0004/0.0006)*	0.204/0.228	0.277/0.202	0.295/0.364
80	20	0.0035/0.0040 *(0.00017/0.00021)*	0.0034/0.0035 *(0.00031/0.00066)*	0.0039/0.0030 *(0.00108/0.00046)*	0.202/0.220	0.270/0.198	0.353/0.308
60	20	0.0025/0.0029 *(0.0002/0.00037)*	0.0027/0.0028 *(0.0004/0.00017)*	0.0022/0.0022 *(0.00043/0.00034)*	0.197/0.215	0.303/0.208	0.302/0.357
40	20	0.0017/0.0021 *(0.00023/0.00003)*	0.0015/0.0018 *(0.00028/0.00034)*	0.0012/0.0012 *(0.00017/0.00017)*	0.208/0.235	0.266/0.199	0.296/0.363
		Cr partial rate coefficient α					
		1.08/1.01	1.13/1.05	1.43/1.53			
		1.09	**1.09**	**1.48**			
100	20	0.0045/0.0052 *(0.00036/0.00071)*	0.0045/0.0045 *(0.00067/0.00064)*	0.0045/0.0047 *(0.0004/0.0006)*	0.204/0.228	0.277/0.202	0.295/0.364
100	15	0.0035/0.0036 *(0.0006/0.0005)*	0.0035/0.0036 *(0.00046/0.00052)*	0.0037/0.0038 *(0.00032/0.00054)*	0.206/0.207	0.293/0.219	0.291/0.328
100	10	0.002/0.002 *(0.00039/0.00039)*	0.0023/0.0020 *(0.00001/0.00021)*	0.0028/0.0029 *(0.0008/0.00059)*	0.169/0.171	0.287/0.244	0.280/0.311
100	5	0.001/0.0012 *(0.00039/0.00001)*	0.0010/0.0014 *(0.0001/0.0001)*	0.0020/0.0022 *(0.00035/0.00031)*	0.157/0.203	0.257/0.316	0.283/0.346
		Mn partial rate coefficient a					
		0.90/0.98	1.00/1.05	0.58/0.53			
		0.94	**1.02**	**0.55**			
					k (averaged) in sec^{-1}		
					pH = 2.5	*pH = 3*	*pH = 3.5*
					0.192/0.211	0.279/0.227	0.300/0.340
					0.201	**0.242**	**0.322**

[a] The partial rate coefficients α, β at pH 2.5, pH 3, and pH 3.5 shown in this table are averaged values from α and β calculated using eqs 6 and 9 and by combining the initial rates measured at different experimental conditions. The rate constant for each experiment was measured with eq 10. Since all experiments were duplicated, the initial rates and rate parameters are reported with two values separated with "/". The standard error (95% confidence interval) for each initial rate is italicized. Averages of duplicate values are highlighted in bold. Reproduced with permission from Landrot et al. Environ. Sci. Technol. *44*, 143–149. Copyright (2010) American Chemical Society.

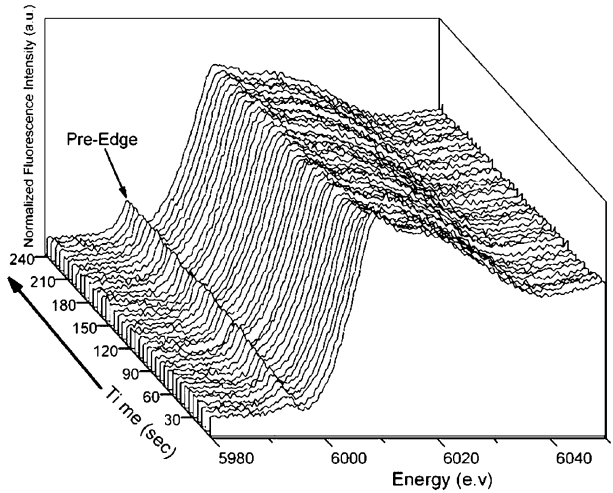

Figure 13. Cr(III) oxidation kinetics using a Q-XAFS technique, at pH 2.5, [Cr(III)] = 100 mM, [HMO] = 20 g/L, and 0−240 s. Each XANES spectrum shown represents 3 s of the reaction (average of four 0.75 s spectra). Reprinted with permission from Landrot et al., Environ. Sci. Technol. 44, 143–149. Copyright (2010) American Chemical Society.

Acknowledgments

The authors gratefully acknowledge the excellent research of former group members, Matthew Ginder-Vogel, Camille Jones, Gautier Landrot, Brandon Lafferty, and Sanjai Parikh, which was reviewed in this chapter.

References

1. Oscarson, D. W.; Huang, P. M.; Defosse, C.; Herbillon, A. The oxidative power of Mn (IV) and Fe (III) oxides with respect to As (III) in terrestrial and aquatic environment. *Nature* **1981**, *291*, 50–51.
2. Shiller, A. M.; Stephens, T. H. Microbial manganese oxidation in the lower Mississippi River: Methods and evidence. *Geomicrobiol. J.* **2005**, *22*, 117–125.
3. Tebo, B. M.; Bargar, J. R.; Clement, B. G.; Dick, G. J.; Murray, K. J.; Parker, D.; Verity, R.; Webb, S. M. Biogenic manganese oxides: Properties and mechanisms of formation. *Annu. Rev. Earth Planet. Sci.* **2004**, *32*, 287–328.
4. Oscarson, D. W.; Huang, P. M.; Hammer, U. T.; Liaw, W. K. Oxidation and sorption of arsenite by manganese dioxide as influenced by surface coatings of iron and aluminum oxides and calcium carbonate. *Water, Air, Soil Pollut.* **1983**, *20*, 233–244.
5. Scott, M. J.; Morgan, J. J. Reactions at oxide surfaces .1. Oxidation of As(III) by synthetic birnessite. *Environ. Sci. Technol.* **1995**, *29*, 1898–1905.

6. Manning, B. A.; Fendorf, S. E.; Bostick, B.; Suarez, D. L. Arsenic(III) oxidation and arsenic(V) adsorption reactions on synthetic birnessite. *Environ. Sci. Technol.* **2002**, *36*, 976–981.
7. Tournassat, C.; Charlet, L.; Bosbach, D.; Manceau, A. Arsenic(III) oxidation by birnessite and precipitation of manganese(II) arsenate. *Environ. Sci. Technol.* **2002**, *36*, 493–500.
8. Chiu, V. Q.; Hering, J. G. Arsenic adsorption and oxidation at manganite surfaces. 1. Method for simultaneous determination of adsorbed and dissolved arsenic species. *Environ. Sci. Technol.* **2000**, *34*, 2029–2034.
9. Petrick, J. S.; Ayala-Fierro, F.; Cullen, W. R.; Carter, D. E.; Aposhian, H. V. Monomethylarsonous acid (MMA(III)) is more toxic than arsenite in Chang human hepatocytes. *Toxicol. Appl. Pharm.* **2000**, *163*, 203–207.
10. Raven, K. P.; Jain, A.; Loeppert, R. H. Arsenite and arsenate adsorption on ferrihydrite: Kinetics, equilibrium, and adsorption envelopes. *Environ. Sci. Technol.* **1998**, *32*, 344–349.
11. Dixit, S.; Hering, J. G. Comparison of arsenic(V) and arsenic(III) sorption onto iron oxide minerals: Implications for arsenic mobility. *Environ. Sci. Technol.* **2003**, *37*, 4182–4189.
12. Moore, J. N.; Walker, J. R.; Hayes, T. H. Reaction scheme for the oxidation of As (III) to As (V) by birnesside. *Clays Clay Miner.* **1990**, *38*, 549–555.
13. Ginder-Vogel, M.; Landrot, G.; Fischel, J. S.; Sparks, D. L. Quantification of rapid environmental redox processes with quick-scanning x-ray absorption spectroscopy (Q-XAS). *Proc. Natl. Acad. Sci. U. S. A.* **2009**, *106*, 16124–16128.
14. Parikh, S. J.; Lafferty, B. J.; Sparks, D. L. An ATR-FTIR spectroscopic approach for measuring rapid kinetics at the mineral/water interface. *J. Colloid Interface Sci.* **2008**, *320*, 177–185.
15. Lafferty, B. J.; Ginder-Vogel, M.; Zhu, M.; Livi, K. J. T.; Sparks, D. L. Arsenite oxidation by a poorly crystalline manganese-oxide. 2. Results from x-ray absorption spectroscopy and x-ray diffraction. *Environ. Sci. Technol.* **2010**, *44*, 8467–8472.
16. Nesbitt, H. W.; Canning, G. W.; Bancroft, G. M. XPS study of reductive dissolution of 7 angstrom-birnessite by H3AsO3, with constraints on reaction mechanism. *Geochim. Cosmochim. Acta* **1998**, *62*, 2097–2110.
17. Tani, Y.; Miyata, N.; Ohashi, M.; Ohnuki, T.; Seyama, H.; Iwahori, K.; Soma, M. Interaction of inorganic arsenic with biogenic manganese oxide produced by a Mn-oxidizing fungus, strain KR21-2. *Environ. Sci. Technol.* **2004**, *38*, 6618–6624.
18. Oscarson, D. W.; Huang, P. M.; Liaw, W. K. Role of manganese in the oxidation of arsenite by freshwater lake sediments. *Clays Clay Miner.* **1981**, *29*, 219–225.
19. Lafferty, B. J.; Ginder-Vogel, M.; Sparks, D. L. Arsenite oxidation by a poorly crystalline manganese-oxide 1. Stirred-flow experiments. *Environ. Sci. Technol.* **2010**, *44*, 8460–8466.
20. Zhu, M. Q.; Paul, K. W.; Kubicki, J. D.; Sparks, D. L. Quantum chemical study of arsenic (III, V) adsorption on Mn-oxides: Implications for arsenic(III) oxidation. *Environ. Sci. Technol.* **2009**, *43*, 6655–6661.

21. Foster, A. L.; Brown, G. E.; Parks, G. A. X-ray absorption fine structure study of As(V) and Se(IV) sorption complexes on hydrous Mn oxides. *Geochim. Cosmochim. Acta* **2003**, *67*, 1937–1953.
22. Peacock, C. L.; Sherman, D. M. Sorption of Ni by birnessite: Equilibrium controls on Ni in seawater. *Chem. Geol.* **2007**, *238*, 94–106.
23. Ramstedt, M.; Shchukarev, A.; Sjoberg, S. Surface properties of manganite (γ-MnOOH). *Geochim. Cosmochim. Acta* **2004**, *68*, A119–A119.
24. Webb, S. M.; Dick, G. J.; Bargar, J. R.; Tebo, B. M. Evidence for the presence of Mn(III) intermediates in the bacterial oxidation of Mn(II). *Proc. Natl. Acad. Sci. U. S. A.* **2005**, *102*, 5558–5563.
25. Perez-Benito, J. F. Reduction of colloidal manganese dioxide by manganese(II). *J. Colloid Interface Sci.* **2002**, *248*, 130–135.
26. Morgan, J. J. Manganese in natural waters and earth's crust: Its availability to organisms. *Met. Ions Biol. Syst.* **2000**, *37*, 1–34.
27. Sparks, D. L. *Kinetics of Soil Chemical Processes*; Academic Press: San Diego, 1989; p xv, 210 pp.
28. Scheidegger, A. M.; Sparks, D. L. A critical assessment of sorption-desorption mechanisms at the soil mineral/water interface. *Soil Sci.* **1996**, *161*, 813–831.
29. Sparks, D. L. *Environmental Soil Chemistry*, 2nd ed.; Academic Press: San Diego, 2002.
30. Landrot, G.; Ginder-Vogel, M.; Sparks, D. L. Kinetics of chromium(III) oxidation by manganese(IV) oxides using quick scanning X-ray absorption fine structure spectroscopy (Q-XAFS). *Environ. Sci. Technol.* **2010**, *44*, 143–149.
31. Siebecker, M.; Li, W.; Khalid, S.; Sparks, D. Real-time QEXAFS spectroscopy measures rapid precipitate formation at the mineral-water interface. *Nat. Commun.* **2014**, *5003*, 1–7.
32. Ginder-Vogel, M.; Stewart, B. D.; Fendorf, S. Kinetic and mechanistic constraints on the oxidation of biogenic uraninite by ferrihydrite. *Environ. Sci. Technol.* **2010**, *44*, 163–169.
33. Sparks, D. L. Advances in the Use of Synchrotron Radiation to Elucidate Environmental Interfacial Reaction Processes and Mechanisms in the Earth's Critical Zone. In *Progress in Soil Science*; Xu, J., Sparks, D. L., Eds.; Springer Science + Business Media: Dordrecht, 2013; pp 93−114.
34. Fendorf, S. E.; Sparks, D. L.; Franz, J. A.; Camaioni, D. M. Electron paramagnetic resonance stopped-flow kinetic study of manganese (II) sorption-desorption on birnessite. *Soil Sci. Soc. Am. J.* **1993**, *57*, 57–62.
35. Dent, A. J. Development of time-resolved XAFS instrumentation for quick EXAFS and energy-dispersive EXAFS measurements on catalyst systems. *Top. Catal.* **2002**, *18*, 27–35.
36. Khalid, S.; Caliebe, W.; Siddons, P.; So, I.; Clay, B.; Lenhard, T.; Hanson, J.; Wang, Q.; Frenkel, A. I.; Marinkovic, N.; Hould, N.; Ginder-Vogel, M.; Landrot, G. L.; Sparks, D. L.; Ganjoo, A. Quick extended x-ray absorption fine structure instrument with millisecond time scale, optimized for in situ applications. *Rev. Sci. Instrum.* **2010**, *81*, 015105.

37. Mitsunobu, S.; Takahashi, Y.; Uruga, T. Observation of chemical reactions at the solid-water interface by quick XAFS combined with a column reactor. *Anal. Chem.* **2006**, *78*, 7040–7043.
38. Ginder-Vogel, M.; Sparks, D. L. The impacts of X-ray absorption spectroscopy on understanding soil processes and reaction mechanisms. In *Developments in Soil Science*; Balwant, S., Markus, G., Eds.; Elsevier: 2010; Vol. 34, pp 1−26.
39. Parikh, S. J.; Chorover, J. ATR-FTIR study of lipopolysaccharides at mineral surfaces. *Colloids Surf., B* **2008**, *62*, 188–198.
40. Lafferty, B. J.; Ginder-Vogel, M.; Sparks, D. L. Arsenite oxidation by a poorly-crystalline manganese oxide. 3. Arsenic and manganese desorption. *Environ. Sci. Technol.* **2011**, *45*, 9218–9223.
41. Parikh, S. J.; Lafferty, B. J.; Meade, T. G.; Sparks, D. L. Evaluating environmental influences on AsIII oxidation kinetics by a poorly crystalline Mn-oxide. *Environ. Sci. Technol.* **2010**, *44*, 3772–3778.
42. Jones, L. C.; Lafferty, B. J.; Sparks, D. L. Additive and competitive effects of bacteria and Mn oxides on arsenite oxidation kinetics. *Environ. Sci. Technol.* **2012**, *46*, 6548–6555.
43. Violante, A.; Pigna, M. Competitive sorption of arsenate and phosphate on different clay minerals and soils. *Soil Sci. Soc. Am. J.* **2002**, *66*, 1788–1796.
44. Luengo, C.; Brigante, M.; Antelo, J.; Avena, M. Kinetics of phosphate adsorption on goethite: Comparing batch adsorption and ATR-IR measurements. *J. Colloid Interface Sci.* **2006**, *300*, 511–518.
45. Roberts, D. R.; Scheidegger, A. M.; Sparks, D. L. Kinetics of mixed Ni-Al precipitate formation on a soil clay fraction. *Environ. Sci. Technol.* **1999**, *33*, 3749–3754.
46. Mihaljevic, M.; Ettler, V.; Sisr, L.; Sebek, O.; Strnad, L.; Vonaskova, V. Effect of low concentrations of phosphate ions on extraction of arsenic from naturally contaminated soil. *Bull. Environ. Contam. Toxicol.* **2009**, *83*, 422–427.
47. Sun, X. H.; Doner, H. E. Adsorption and oxidation of arsenite on goethite. *Soil Sci.* **1998**, *163*, 278–287.
48. Feng, X. J.; Simpson, A. J.; Simpson, M. J. Investigating the role of mineral-bound humic acid in phenanthrene sorption. *Environ. Sci. Technol.* **2006**, *40*, 3260–3266.
49. He, Y. T.; Hering, J. G. Enhancement of arsenic(III) sequestration by manganese oxides in the presence of iron(II). *Water, Air, Soil Pollut.* **2009**, *203*, 359–368.
50. Peterson, M. L.; Brown, G. E., Jr.; Parks, G. A. Direct XAFS evidence for heterogeneous redox reaction at the aqueous chromium/magnetite interface. *Colloids Surf., A* **1996**, *107*, 77–88.
51. Peterson, M. L.; Brown, G. E.; Parks, G. A.; Stein, C. L. Differential redox and sorption of Cr(III/VI) on natural silicate and oxide minerals: EXAFS and XANES results. *Geochim. Cosmochim. Acta* **1997**, *61*, 3399–3412.
52. Sparks, D. L. Kinetics of Soil Chemical Phenomena: Future Directions. In *Future Prospects for Soil Chemistry*; Huang, P. M., Sparks, D. L., Boyd, S. A., Eds.; SSSA: Madison, WI, 1998; Special Publication no. 55, pp 81−101.

53. Fendorf, S. E. Surface reactions of chromium in soils and waters. *Geoderma* **1995**, *67*, 55–71.
54. Gray, M. J.; Malati, M. A. The point of zero charge of manganese dioxides. *J. Electrochem.* **1978**, *89*, 135–140.
55. Fendorf, S. E.; Fendorf, M.; Sparks, D. L. Inhibitory mechanisms of Cr(III) oxidation by δ-MnO2. *J. Colloid Interface Sci.* **1992**, *153*, 37–54.
56. Eary, E.; Rai, D. Kinetics of chromium(III) oxidation to chromium(VI) by reaction with manganese dioxide. *Environ. Sci. Technol.* **1987**, *21*, 1187–193.
57. Manceau, A.; Charlet, L. X-ray adsorption spectroscopy study of the sorption of Cr(III) at the oxide-water interface. I. Molecular mechanism of Cr(III) oxidation on Mn Oxides. *J Colloid Interface Sci.* **1992**, *148*, 425–442.
58. Weaver, R. M.; Hochella, M. F. The reactivity of seven Mn-Oxides with Cr^{3+}_{aq}: a comparative analysis of a complex, environmentally important redox reaction. *Am. Mineral.* **2003**, *88*, 2016–2028.
59. Kim, J. G.; Dixon, J.; Chusui, C. C.; Deng, Y. Oxidation of chromium(III) to (VI) by manganese oxides. *Soil Sci. Soc. Am. J.* **2002**, *66*, 306–316.
60. Tang, Y.; Webb, S. W.; Estes, R. E.; Hansel, M. C. Chromium(III) oxidation by biogenic manganese oxides with varying structural ripening. *Enivron. Sci.: Processes Impacts* **2014**, *16*, 2127–2136.
61. Kim, J. G.; Moon, H. S. Oxidation of chromium (III) to chromium (VI) by a series of synthesized birnessites (δ-MnO2): kinetics and oxidation capacity. *Clay Sci.* **1998**, *10*, 363–374.
62. Johnson, A. C.; Xyla, A. G. The oxidation of chromium(III) to chromium(VI) on the surface of manganite (γ-MnOOH). *Geochim. Cosmochim. Acta* **1991**, *55*, 2861–2866.
63. Banerjee, D.; Nesbitt, H. W. Oxidation of aqueous Cr(III) at birnessite surfaces: constraints on reaction mechanism. *Geochim. Cosmochim. Acta* **1999**, *63*, 1671–1687.
64. Nico, P.; Zasoski, R. Importance of Mn(III) availability on the rate of Cr(III) oxidation on δ-MnO2. *Environ. Sci. Technol.* **2000**, *34*, 3363–3367.
65. Rai, D.; Sass, B.; Moore, D. Chromium(III) hydrolysis constants and solubility of chromium(III) hydroxide. *Inorg. Chem.* **1987**, *26*, 345–349.
66. Fendorf, S. E.; Zasoski, R. J. Chromium(III) oxidation by δ-MnO2 1. Characterization. *Environ. Sci. Technol.* **1992**, *26*, 79–85.
67. Feng, X. H.; Zhai, L. M.; Tan, W. F.; Zhao, W; Liu, F.; He, J. Z. The controlling effect of pH on oxidation of Cr(III) by manganese oxide minerals. *J. Colloid Interface Sci.* **2006**, *298*, 258–266.
68. Dai, R. A.; Liu, J.; Yu, C. Y.; Sun, R.; Lan, Y. Q.; Mao, D. J. A comparative study of oxidation of Cr(III) in aqueous ions, complex ions and insoluble compounds by manganese-bearing mineral (birnessite). *Chemosphere* **2009**, *76*, 536–541.
69. Landrot, G.; Ginder-Vogel, M.; Livi, K.; Fitts, J. P.; Sparks, D. L. Chromium(III) oxidation by three poorly-crystalline manganese(IV) oxides. 1. Chromium(III)-oxidizing capacity. *Environ. Sci. Technol.* **2012**, *46*, 11595–11600.